A&A 460, 733–741 (2006)
DOI: 10.1051/0004-6361:20065873

Astronomy & Astrophysics

Search for cold debris disks around M-dwarfs

J.-F. Lestrade[1], M. C. Wyatt[2], F. Bertoldi[3], W. R. F. Dent[4], and K. M. Menten[5]

[1] Observatoire de Paris – CNRS, 77 Av. Denfert Rochereau, 75014 Paris, France
e-mail: jean-francois.lestrade@obspm.fr
[2] Institute of Astronomy, University of Cambridge, Cambridge, CB3 OHA, UK
e-mail: wyatt@ast.cam.ac.uk
[3] Radioastronomisches Institut, Universität Bonn, Auf dem Hügel 71, Bonn 53121, Germany
e-mail: bertoldi@astro.uni-bonn.de
[4] UK Astronomy Technology Center, Royal Observatory, Observatory, Edinburgh, EH9 3HJ, UK
e-mail: dent@roe.ac.uk
[5] Max-Planck-Institut für Radioastronomie, Auf dem Hügel 69, Bonn 53121, Germany
e-mail: kmenten@mpifr-bonn.mpg.de

Received 21 June 2006 / Accepted 15 September 2006

ABSTRACT

Debris disks are believed to be related to planetesimals left over around stars after planet formation has ceased. The frequency of debris disks around M-dwarfs which account for 70% of the stars in the Galaxy is unknown while constrains have already been found for A- to K-type stars. We have searched for cold debris disks around 32 field M-dwarfs by conducting observations at $\lambda = 850$ μm with the SCUBA bolometer array camera at the JCMT and at $\lambda = 1.2$ mm with the MAMBO array at the IRAM 30-m telescopes. This is the first survey of a large sample of M-dwarfs conducted to provide statistical constraints on debris disks around this type of stars. We have detected a new debris disk around the M0.5 dwarf GJ 842.2 at $\lambda = 850$ μm, providing evidence for cold dust at large distance from this star (~300 AU). By combining the results of our survey with the ones of Liu et al. (2004), we estimate for the first time the detection rate of cold debris disks around field M-dwarfs with ages between 20 and 200 Myr. This detection rate is 13^{+6}_{-8}% and is consistent with the detection rate of cold debris disks (9–23%) around A- to K-type main sequence stars of the same age. This is an indication that cold disks may be equally prevalent across stellar spectral types.

Key words. stars: circumstellar matter

1. Introduction

In star-forming regions, a large fraction of the M-type low-mass stars younger than 6 Myr have disks of gas and dust that are primordial materials for planet formation (Beckwith et al. 1990; Haisch et al. 2001; Dutrey et al. 1996; Andrews & Williams 2005; Muzerolle et al. 2006). However, little is known about the frequency of planetary systems around mature M-type dwarfs (ages > 10 Myr) that account for 70% of the stars in the Galaxy. For example, amongst the ~170 stars hosting planets discovered by the radial velocity technique, only three are M-dwarfs (GJ 876 (Marcy et al. 2001), GJ 436 (Butler et al. 2004), and GJ 581 (Bonfils et al. 2005). This paucity may be due to selection effects because M-dwarfs are optically faint and chromospherically active, making radial velocity measurements more difficult than for solar-type stars (Endl et al. 2003). From microlensing events, it has been infered that many M-dwarfs have planets with masses smaller than Jupiter. However this inference is based on statistical arguments from a small number of events (Gaudi et al. 2002 and Beaulieu et al. 2006).

Another approach to estimate the frequency of planetary systems around stars is to measure the frequency of debris disks around them. A debris disk is made of planetesimals left over from the planetary formation processes. In these disks, dust grains are continuously regenerated by collisions and/or evaporation of the planetesimals. This dust absorbs stellar radiation at visual wavelengths and reradiates the energy at infrared (IR) to submillimeter (sub-mm) wavelenghts. It is the large emitting surface area of these numerous grains that makes debris disks around stars observable in the IR and sub-mm, while the mass-dominant planetesimals remain undetected. IR to sub-mm excesses above photospheric emissions of a few hundreds main sequence A- to K-type dwarfs have been photometricly detected by IRAS (Aumann et al. 1984; Walker & Wolstenscroft 1988; Backman & Paresce 1993; Mannings & Barlow 1998), by ISO (Habing et al. 2001; Spangler et al. 2001; Laureijs et al. 2002), and by Spitzer (Rieke et al. 2005; Beichman et al. 2005; Chen et al. 2005; Bryden et al. 2006). Futhermore, imaging of the emitting dust in the (sub)mm of a few debris disks has revealed substructures that are best interpreted as dust trapped in resonance with an unseen planet in the inner part of the system (Wyatt 2003, 2006). Also the large reflecting surface area of the dust grains is responsible for scattered light that provides a wealth of information useful to disclose the structure and dynamics of these systems (e.g. β Pic in Golimowski et al. 2006). Cold dust in the Kuiper Belt and warm dust in the asteroid belt are the debris of our solar system.

The first attempt to search for mid-IR excesses from field M-dwarfs, i.e. M-stars outside of star forming regions, yielded only three detections in the IRAS point source catalogue (Inseok Song et al. 2002). However, debris disks around M-dwarfs may be missed by such mid-IR surveys because M-dwarfs are underluminous ($L = 0.1$–0.001 $L_\odot$) so that the irradiated dust is cold (<20 K) and more easily detected at (sub)mm wavelengths. In this paper, we report on observations of 32 young

Table 1. JCMT/SCUBA wide photometry at 850 μm.

Star	Sp. type	RA[a] (J2000)	Dec[a] (J2000)	Dist. (pc)	Log (L_x)[b] Log (erg/s)	Moving Group	Integration time (h)	Flux density (mJy)	Size [c] (AU)	Dust temp[d] (K)	Dust mass[e] (moon)
GJ 82	M4	01 59 23.5	58 31 16	12.0	28.75	Loc Ass.	2	2.0 ± 1.4	84	16	<1.3
GJ 212	M0.5	05 41 30.7	53 29 20	12.5	28.57	Loc Ass.	2	1.3 ± 1.4	88	23	<0.8
GJ 285	M4.5	07 44 40.1	03 33 08	5.9	28.62	Loc Ass.	1	–0.7 ± 1.9	41	20	<0.3
GJ 393	M2	10 28 55.5	00 50 27	7.2	26.84	Loc Ass.	1	1.9 ± 1.9	50	26	<0.3
GJ 507.1	M1.5	13 19 40.1	33 20 47	17.4	n/a	Loc Ass.	1	–0.4 ± 2.0	121	19	<2.8
GJ 696	M0	17 50 34.0	–06 03 01	21.9	n/a	Loc Ass.	2	0.8 ± 0.8	150	20	<1.9
GJ 9809	M0	23 06 04.8	63 55 34	24.9	29.43	Loc Ass.	1	–5.2 ± 2.3	174	18	<7.6
GJ 4247	M4	22 01 13.2	28 18 25	9.0	n/a	Castor	1	1.1 ± 2.1	63	18	<0.9
GJ 277B	M3.5	07 31 57.3	36 13 47	11.5	29.05	Castor	1	–2.1 ± 1.8	80	17	<1.3
GJ 842.2	M0.5	21 58 24.8	75 35 21	20.9	n/a	Castor	4	25 ± 4.6[f]	300	13	28 ± 5
GJ 890	M2	23 08 19.5	–15 24 35	21.9	29.22	Castor	2	–2.6 ± 1.6	153	16	<4.5
GJ 875.1	M3	22 51 53.7	31 45 15	14.2	28.92	IC2391	1	0.52 ± 2.1	99	17	<2.4

[a] Observed positions, i.e. coordinates updated with the Hipparcos proper motions at the mean observation date of September 2004.
[b] ROSAT All Sky Survey of Nearby Stars: Huensch et al. (1999).
[c] Size is the radius of a debris disk as large as the telescope beam (14″).
[d] Temperature is computed at this radius.
[e] Mass upper limits are based on the 3σ flux densities (see text).
[f] Total flux density of the extended emission and the South-West peak.

field M-dwarfs at λ = 850 μm with the Submillimeter Common User Bolometer Array (SCUBA) at the James Clerk Maxwell Telescope (JCMT), and at λ = 1.2 mm with the Max-Planck Millimeter Array (MAMBO) at the IRAM 30 m telescope. Previously, only three field M-dwarfs have been observed in the (sub)mm (Liu et al. 2004). Our aim is to determine the frequency of debris disks around M-dwarfs.

Several studies have adressed the problem of planet formation around M-dwarfs and their associated debris disks. Mechanisms that might be specific to this stellar spectral type have been discussed by Johnstone et al. (1998), Laughlin et al. (2004), Throop & Bally (2005), Plavchan et al. (2005). Our contribution to establishing the statistics of debris disks around M-dwarfs provides new observational constrains.

Section 2 briefly describes the target stars. Section 3 describes the observations at the JCMT and IRAM30 m (sub)mm telescopes. Section 4 describes the results of these observations and provides details on the discovery of the debris disk around the M0.5 dwarf GJ 842.2. We draw statistical conclusions on debris disks around M-dwarfs in Sect. 5.

2. Target stars

Observations have shown that debris disks around main sequence stars of spectral types A to K with ages less than 150–400 Myr are dustier than older ones (Habing et al. 2001, Rieke et al. 2005). We therefore selected the youngest M-dwarfs in their post planetary formation phase with ages older than 10 Myr. We shall not denote them main-sequence stars because an M0 star, e.g., reaches the main sequence only after 900 Myr (Siess et al. 2000). We selected the M-dwarfs that belong to the Moving Groups identified by Montes et al. (2001) and Zuckerman & Inseok Song (2004a,b), since membership to such a group is a reliable age criterium. The selected stars belong to the Local Association open cluster (age = 20–150 Myr), IC2391 (35–55 Myr), the AB Dor moving group (100–125 Myr as revised by Luhman et al. 2005), the Castor moving group (200 Myr), the Ursa Maj moving group (500 ± 100 Myr as revised by King et al. 2003), and the Hyades open cluster (600 Myr). Note that HIP114066 is part of the AB Dor group according to Zuckerman & Inseok Song (2004a,b) but is named GJ 9809 and assigned to the Local Association by Montes et al. (2001). In our surveys, the completness for M-dwarfs in the Local Association is 61% (11 M-dwarfs observed/18 M-dwarfs in cluster), in Castor it is 75% (6/8), in Ursa Major it is 40% (4/10), in AB Dor it is 71% (5/7), in Hyades it is 29% (5/17), in IC2391 it is 50% (1/2). The M-dwarfs of these clusters that are not included in our surveys were inaccessible to the telescopes because of their low declinations. The selected stars have distances between 2.6 pc and 33.8 pc. Our surveys at λ =1.2 mm and 850 μm include the observations of 32 different stars; 12 were observed at the JCMT and 24 at the IRAM 30 m telescope with four stars in common in the two surveys (GJ 285, GJ 393, GJ 9809, GJ 4247).

3. Observations

3.1. JCMT/SCUBA observations

The SCUBA bolometer array (Holland et al. 1999) at the JCMT in Hawaii at altitude 4092 m was used to observe the 12 M-dwarfs listed in Table 1. SCUBA uses two arrays of 37 and 91 bolometers to simultaneously observe at 850 μm and 450 μm, respectively, the same region of the sky which is ∼2.3′ in size. The arrays are arranged as concentric hexagonal rings of bolometers at each wavelength. A fully sampled map of the 2.3′ region can be made by "jiggling" the arrays according to an optimized pattern (Holland et al. 1999) but requires a long integration time to reach the 2 mJy/14″ beam sensitivity sought in our program. Standard photometry with a single bolometer of the array (i.e. on-off observations for sky background substraction) yields sensitive observations in less time but the target source must be smaller than the beam (*FWHM* = 14″ at 850 μm). This is not certain for most of our targets because of the large a priori uncertainty on disk sizes (factor 3–5). Thus, in order to optimize the use of our observing time, SCUBA data were taken in the *wide photometry* mode of JCMT described by Sheret et al. (2004). It ensures that a source that is partially resolved or offset from the observed position is detected with maximum sensitivity. In practice, the arrays are moved through a 12-point pattern

that makes the central bolometer of each array cycles through 4 inner points at 1″ from the target position and 8 outer points at 7″.

In general, an observation consisted of 78 integrations of 38 seconds, which corresponds to the total on+off time of 50 min. During each integration, the telescope beam cycled through the 12-point pattern described above and the secondary mirror continuously chopped the sky over 60″ at 7.8125 Hz in azimuth to remove any large-scale sky variations. Each observation of a target was preceded and followed by focusing and pointing. Atmospheric opacity $\tau_{225\ \mathrm{GHz}}$ was measured by radiometry several times per minute and by "skydips" once every few hours; $\tau_{225\ \mathrm{GHz}}$, the zenith opacity at 225 GHz, the operating frequency of the radiometer, was between 0.06 and 0.08 during our observations, corresponding to precipitable water vapour columns of ∼1.2–1.6 mm. The absolute flux density scale was checked by 11 measurements of standard calibrators at 850 μm (Uranus, Saturn, CRL 2688, CRL 618) over the 7 sessions of our program between August 26 2004 and October 07 2004. From these measurements, we derived a conversion factor $FCF = 222 \pm 15$ (Jy/Volt) for this period. The uncertainty in this factor provides the accuracy of our absolute flux density scale, which is better than 10% at 850 μm. Observations at 450 μm are ∼15 times less sensitive than at 850 μm while the flux density is only 6 times higher for dust with a modified blackbody spectrum and $\beta = 1$. None of our targets were detected at this shorter wavelength.

The SURF package (Jenness et al. 2002) was used to combine the data from different integrations, remove anomalous spikes, flatfield the array, subtract the sky-background noise level and apply atmospheric extinction corrections. The calibrated data were then analysed by a specific software to average the data of the central bolometer and to produce the map with the data of all the bolometers. This map is incomplete however because the sky is undersampled in the wide photometry mode. Nonetheless it allows to realiably detect a source, although interpretation of its measured flux density and morphology is somewhat complicated. For the two sources detected (GJ 842.2 and GJ 696), we also re-analysed the data with the Edinburgh custom data-reduction software written in IDL and found similar results. The observations of the 12 M-dwarfs were conducted on 2004 August 26, 29, 31, on 2004 September 19 and on 2004 October 3, 6, 7. In the course of this programme, GJ 842.2 was observed 4 times, GJ 82, GJ 212, GJ 696, and GJ 890 twice and the other stars once.

3.2. IRAM 30 m/MAMBO observations

The 117-channel MPIfR bolometer array MAMBO-2 (Kreysa et al. 1998) at the IRAM 30-m telescope on Pico Veleta at 2900 m altitude near Granada in Spain was used to observe the 24 M-dwarfs listed in Table 2. MAMBO-2 operates at an effective frequency of 250 GHz ($\lambda = 1.20$ mm) with a half-power spectrum bandwidth of 80 GHz. At $\lambda = 1.20$ mm, the IRAM 30-m telescope has an effective beam of 10.7″(*FWHM*), smaller than the angular sizes of the potential debris disks for most of our targets. Simple on-off photometry pointed at the target would therefore not be a good strategy to detect a disk and multiple pointed observations, similar to wide photometry at JCMT, would be inefficient at the IRAM 30-m telescope because of the overhead due to the motion of this large telescope. Thus, we mapped the targets.

We used the standard on-the-fly scanning mode, where the telescope scans in the azimuthal direction. The signal from the sky was modulated by the secondary mirror wobbling over a throw of 60″ at 2 Hz in the scan direction (azimuth). The wobble frequency reflects a compromise between eliminating changes in the atmosphere on as short a time-scale as possible and the challenges involved in moving a 2-m secondary at this frequency and keeping it mechanically stable. For each target, we made a map, 400×320 arcsec^2 in size, scanned at a velocity of 4 arcsec s^{-1} and with an elevation spacing of 4 arcsec. This results in a fully-sampled map over this area with a ∼2 mJy/11″ beam rms noise in the central region per observation of 33 min (on + off times). Some targets were observed twice or more in different scan directions and maps were co-added to improve this rms noise. In practice, however, weather conditions for these multiple observations were different (opacity $0.2 < \tau_{225\ \mathrm{GHz}} < 0.45$, low and medium sky-background noise) and thus, quite often, one of the maps dominates the final summation (except for GJ 628). The opacity of the atmosphere was measured every other hour by performing a skydip, but was also continuously monitored with a radiometer located next to the telescope. Short on-off observations of position calibrators were carried out before and after each observation of the programm sources to check the telescope pointing which was found to be excellent (∼1″). In order to set the absolute flux density scale, primary flux calibrators (including planets) were observed at the beginning and end of each run, which resulted in an absolute flux calibration uncertainty of ∼15% (1σ).

The IRAM data were reduced using the MOPSIC software package (Zylka 1998). Data were despiked, filtered for atmospheric variations, flat-fielded and corrected for atmospheric opacity and turned into intensity maps and signal-to-noise ratio maps. The observations of the 24 M-dwarfs listed in Table 2 were conducted in December 2004, in January, February and May 2005, and in January and March 2006. Integration times were between 0.5 and 2 h (see Table 2). GJ 628 has been a special case, after detecting possibly significant peaks in the first maps, we extended our observations to 20 h of integration to reach a map noise rms of 0.4 mJy/11″ beam in order to search for diffuse emission between these peaks.

The relevant sensitivities for our SCUBA and MAMBO surveys are in terms of circumstellar dust mass rather than mJy. Although the sensitivity is ∼2 mJy/beam for each observations in both surveys, the sensitivity with MAMBO was enhanced by taking a higher number of observations and by averaging the data over a canonical disk area assumed as large as the Kuiper-belt. This averaging can be done also with the SCUBA wide photometry data but not as efficiently because the sky is not fully sampled. Also the dust mass sensitivity depends on the stellar distance squared, and the M-dwarfs observed with MAMBO are closer than the ones observed by SCUBA in general. The all-in sensitivity is ∼1 lunar mass of circumstellar dust for both surveys.

4. Results

4.1. JCMT/SCUBA results

In our JCMT/SCUBA sample of 12 M-dwarfs, we have detected significant peaked and extended emissions around GJ 842.2 revealing a debris disk around this M0.5 dwarf. We analysed the data of GJ 842.2 in two ways. First, we straightforwardly averaged the data of the central bolometer and made a significant detection with a flux density of 4.8 ± 1.3 mJy. In effect, this flux density is the average of the emission at the 4 points 1″ away from the star position and at the 8 points 7″ away and may

Table 2. IRAM/MAMBO aperture photometry at $\lambda = 1.2$ mm.

Star	Sp. type	RA[a] (J2000)	Dec[a] (J2000)	Dist. (pc)	Log (L_x)[b] Log (erg/s)	Moving group	Integr. time (h)	θ ($''$)	Mean brightness[c] (mJy/11$''$ beam)	Map noise rms (mJy/11$''$ beam)	F_θ^d (3σ) (mJy)	Dust temp.[e] (K)	Dust mass[f] (moon)
GJ 65A	M5.5	01 39 02.6	–17 56 59	2.6	27.59	Hyades	1.1	46	-0.30 ± 0.5	2.1	26	15	<0.9
GJ 109	M3	02 44 15.8	25 31 22	7.6	27.30	Hyades	1.3	16	0.67 ± 1.4	2.1	9	21	<1.6
HIP 16563B[g]	M0	03 33 14.0	46 15 19	33.8	n/a	AB Dor	0.9	4	0.35 ± 1.0[h]	–	3	27	<8.0
HIP 17695	M3	03 47 23.4	–01 58 21	16.3	n/a	AB Dor	0.5	5	-0.79 ± 2.2	2.2	7	20	<5.6
GJ 3379	M4	06 00 04.5	02 42 23	5.4	n/a	Hyades	0.5	22	-0.06 ± 1.1	2.3	14	18	<1.5
GJ 234A	M4	06 29 23.6	–02 48 53	4.1	n/a	Loc Ass	1.1	29	0.76 ± 0.7	1.8	14	18	<0.9
GJ 285	M4.5	07 44 40.0	03 33 06	5.9	28.62	Loc Ass	1.1	20	-0.13 ± 1.0	1.7	9	17	<1.1
GJ 1111	M6.5	08 29 49.1	26 46 29	3.6	n/a	Castor	0.5	33	-0.34 ± 0.8	2.4	22	12	<1.9
GJ 393	M2	10 28 55.3	00 50 24	7.2	26.84	Loc Ass	1.7	18	-0.38 ± 1.1	1.5	7	24	<0.8
GJ 402	M4	10 50 51.8	06 48 25	6.8[i]	n/a	Loc Ass	1.1	18	-0.24 ± 1.0	1.7	8	18	<1.0
GJ 447	M4	11 47 44.5	00 48 10	3.3	26.84	Ursa Ma	1.1	36	0.28 ± 0.4	1.4	14	18	<0.6
GJ 408	M2.5	11 00 04.1	22 49 57	6.6	26.60	Castor	1.1	18	0.16 ± 1.0	1.7	8	22	<1.0
GJ 569A	M2	14 54 29.3	16 06 03	9.8	28.54	Ursa Ma	1.1	12	1.76 ± 2.2	2.2	7	24	<1.8
GJ 628	M3.5	16 30 18.0	–12 39 51	4.3	26.48	Loc Ass	20.0	28	0.1 ± 0.2	0.4	3	12	<0.4
GJ 625	M1.5	16 25 24.8	54 18 13	6.6	26.70	Ursa Ma	0.5	18	-0.85 ± 1.5	2.5	12	26	<1.3
HIP 81084	M0.5	16 33 41.5	–09 33 12	31.9	n/a	AB Dor	0.5	4	0.63 ± 2.6	2.6	8	27	<19
HIP 86346	M0	17 38 39.6	61 14 16	24.5	n/a	AB Dor	0.5	5	-0.13 ± 2.1	2.1	6	27	<8.2
GJ 791.2	M4.5	20 29 48.6	09 41 19	8.9	27.89	Hyades	1.1	14	-0.98 ± 1.7	1.7	6	17	<2.0
GJ 849	M3.5	22 09 40.7	–04 38 26	8.8	n/a	Hyades	0.5	14	-1.32 ± 2.7	2.7	10	19	<2.7
GJ 876	M4	22 53 17.0	–14 15 52	4.7	n/a	Loc Ass	0.5	25	-0.07 ± 1.5	2.8	19	18	<1.6
GJ 873	M3.5	22 46 49.3	44 19 59	5.0	29.09	Ursa Ma	0.6	24	0.32 ± 1.1	2.0	13	19	<1.1
GJ 4247	M4	22 01 13.2	28 18 25	9.0	n/a	Castor	1.1	13	-0.18 ± 1.4	1.4	5	18	<1.5
GJ 856A	M3	22 23 29.1	32 27 32	16.1	29.46	AB Dor	1.1	8	-0.56 ± 1.5	1.5	4	21	<3.3
GJ 9809	M0	23 06 04.8	63 55 34	24.9	29.43	Loc Ass	0.5	7	0.36 ± 2.2	2.2	7	26	<10

[a] Observed positions, i.e. coordinates updated with the Hipparcos proper motions at the mean observation date of July 2005.
[b] ROSAT All Sky Survey of Nearby Stars: Huensch et al. 1999.
[c] Mean brightness computed over the effective area of angular size $\theta(''$) corresponding to the canonical disk 120 AU in diameter.
[d] Total flux density F_θ is the 3σ map noise integrated over this canonical disk.
[e] Dust temperature computed at 60 AU from the central star.
[f] Dust mass upper limits based on F_θ.
[g] Designation and spectral type from Zuckerman & Inseok Song (2004b) and López-Santiago et al. (2006).
[h] On-off single bolometer MAMBO standard photometry.
[i] Based on parallax from the Research Consortium on Nearby Stars RECONS project (`www.chara.gsu.edu/RECONS`).

be underestimated depending on the morphology of the source (Sheret et al. 2004). Nonetheless, the source is detected and this is the important point for the survey. Second, we averaged the data from the first ring of bolometers (6 bolometers at mean radius 25$''$ from center), and found the significant mean brightness of 2.4 ± 0.6 mJy/14$''$ beam over this area. We have also averaged the data of the second ring of bolometers further away at 45$''$ and found 0.83 ± 0.70 mJy/beam, i.e., consistent with no detection. The third ring at 65$''$ was used to remove sky-background noise and, thus, defines the zero-level of the flux density scale. This implies that extended emission exists out to ~25$''$ and so the emitting disk is as large as ~500 AU at the distance of GJ 842.2 (20.9 pc). In an attempt to identify the general morphology of this extended emission, we split the field of view in eight sectors to average the data in each one of them (Fig. 1). In this decomposition, we used only two free parameters, the global orientation of the sectors and the arclength of the inner South-West sector, maximizing the signal-to-noise ratio in it. The sector radii are not free parameters but imposed by the SCUBA array. This averaging of the data indicates that the emission is non-uniformly distributed and is oriented along the North East-South West direction, suggesting an inclined disk. The plot at the bottom of Fig. 1 is a section of the brightness along this direction. The total flux density (brightness × surface area) is estimated to be $\sim 25 \pm 4.6$ mJy (i.e. $S/N = 5.5$) by adding the flux densities of the 4 sectors along the Norh East-South West direction. Finally, we computed the likelihood that the offset peak corresponding to the South-West sector (~11 mJy at 7$''$) is a background source. The probability to find a background source within a radius of 7$''$ from an observed position in our 12 star survey is as low as 3%, computed from $2100 \times (11/2.3)^{-1.5} \times \pi(7''/3600'')^2 \times 12$, based on the source count power-law $N(S) \propto S^{-1.5}$ normalized by 2100 sources/deg^2 for $S > 2.3$ mJy at 850 μm (Rowan-Robinson 2001). So we conclude that there is a cold debris disk around GJ842.2, possibly inclined, made of a peak of emission at 7$''$ South West from the star (~140 AU at 20.9 pc) embedded in low brightness emission extending over 25$''$ (~500 AU). We emphasize that this attempt to identify the general morphology of the disk is speculative and that the straightforward averaging of the data of the first ring of bolometers mentioned above that indicates an extended source of mean brightness 2.4 ± 0.6 mJy/14$''$ beam is our main result.

The total SCUBA flux density $S_{850\,\mu\mathrm{m}}$ of GJ 842.2 was used to calculate the dust mass M_d of the disk by assuming a simple model of large grains (100 μm in size) located at the mean radius of the extended disk (300 AU). We use the standard optically thin dust formula for (sub)mm emission ($S_\lambda = M_\mathrm{d} \times B(\lambda, T_\mathrm{g}) \times \kappa_\mathrm{abs}/d^2$, where T_g is the grain temperature, d is the star distance, $\kappa_\mathrm{abs} = \kappa_{850\,\mu\mathrm{m}} \left(\frac{850\,\mu m}{\lambda}\right)^\beta$ is the mass opacity for the modified black body, with $\kappa_{850\,\mu\mathrm{m}} = 1.7$ cm^2 g^{-1} and $\beta = 0.8$ for ~100 μm size grains, Dent et al. 2000). At 300 AU, the dust temperature is only 13 K and the total dust mass is 28 ± 5 lunar

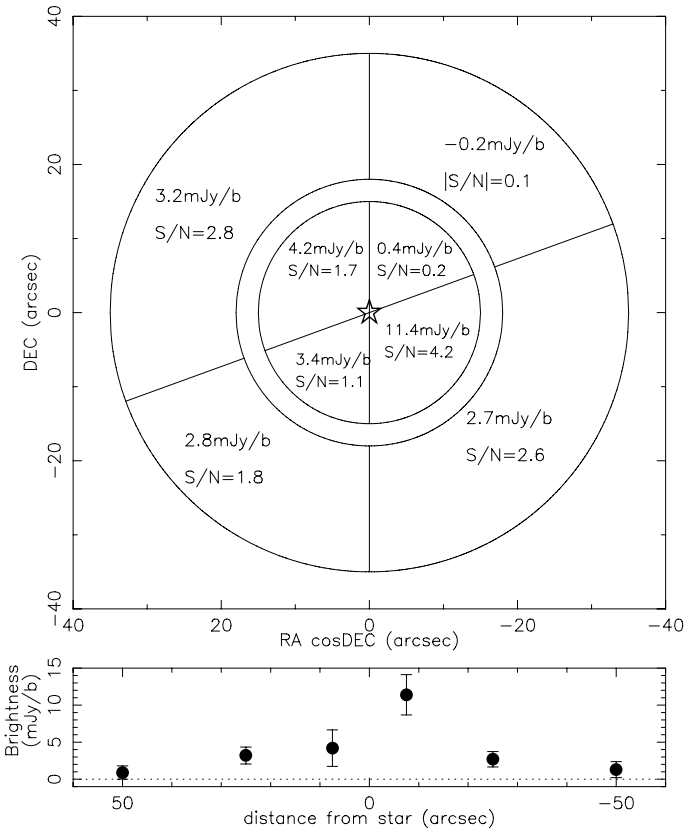

Fig. 1. Brightness distribution around the M0.5 dwarf GJ842.2 at λ = 850 μm based on the data from all the bolometers of the JCMT/SCUBA array. We made an attempt to identify the general morphology of the source in splitting the field of view in eight sectors and averaging the data in each one of them. As it is seen, the emission is non-uniformly distributed and is oriented along the North East-South West direction, suggesting an inclined disk. The plot at the bottom of the figure is a section of the brightness along this direction. The total flux density (brightness × surface area) is estimated to be ∼25 ± 4.6 mJy (i.e. S/N = 5.5) by adding the flux densities of the 4 quadrants along this direction. The *FWHM* beamwidth of the telescope is 14″ at 850 μm. Observed position of GJ 842.2 is α = 21h58 m 24.8 s and δ = 75°35′21″ (J 2000).

masses for $S_{850\,\mu m}$ = 25 ± 4.6 mJy. Those simple assumptions provide only the magnitude of the cold dust mass for the disk of GJ 842.2 but it shows clearly that it is larger than the dust mass estimated around the M1 dwarf AU Mic (∼1 lunar mass) and around the M0.5 dwarf GL182 (∼2.1 lunar mass) by Liu et al. (2004).

In addition, we reanalysed IRAS data of GJ 842.2 with the on-line program *scanpi* and determined the color-corrected flux density 57 ± 12 mJy at 12 μm. This flux density matches the photospheric emission computed from the NextGen model for this M0 dwarf ($T_{\rm photo}$ = 3500 K, g = 5.5, [Fe/H] = 0.0) by Allard et al. (2000, 2001), normalized by the *B, V, R, I, J, H, K* flux densities of GJ 842.2 accessible in the SIMBAD data base (*B*, *V* bands: Third Catalogue of Nearby Stars (1991) by Gliese and Jahreiss, Astron. Rechen-Institut, Heidelberg; *B, R, I* bands: USNO-B1.0 catalogue, Monet et al. 2003; *J, H, K* bands: 2MASS All-Sky catalogue of point sources, Skrutskie et al. 2006). The scanpi signals in the other IRAS bands were not significant except possibly at 25 μm (58 ± 13 mJy, color corrected). However, an IRAS flux density must be treated circumspectly when the signal-to-noise ratio is lower than 5. If this 25 μm flux density (4.5σ) were real however, it would be clearly higher than the photospheric level of GJ 842.2 and so, interestingly, indicative of warm dust close to the star. This needs confirmation by new observations.

For the M0.5 dwarf GJ 696 in our survey, the central bolometer data did not yield any significant flux density in the central region close to this star (radius <14″) and data averaging of the first ring of bolometers (18″–35″) did not reveal any extended emission at the 1σ level of 0.8 mJy/14″ beam. However, we have found a significant peak of emission, 11 mJy (4σ) at 20.8″ and PA = +73° (East-North-East) from the position of this star in the SCUBA incomplete map. It it is possible that its true flux density is underestimated because of undersampling as mentioned above. This peak is 10 times higher than the noise of the first ring of bolometers. Thus, we do not regard this detection as evidence for a debris disk around GJ 696, referring to the SCUBA map of ϵ Eri which shows ratio between peaks and diffuse emission of less than 2 (Greaves et al. 2005). It is likely that the peak near GJ 696 is a background source. We computed the likelihood a sub-mm background source be within a radius of 21″ over the whole 12 star sample using the source count at 850 μm by Rowan-Robinson (2001) and found a probability of 25%. There is no corresponding 1.4 GHz radio counterpart in the NVSS catalogue by Condon et al. (1998) and no optical object in the USNO-B1 catalogue that is positionally coincident.

No peaked or diffuse emissions have been detected around the other 10 stars of our survey. In Table 1, we derived the upper limits on the dust masses of their potential debris disks using the 3σ flux density upper limits and the dust temperature for a linear separation from the star corresponding to 7″ which is the angular extent well probed by wide photometry.

4.2. IRAM 30 m/MAMBO results

In our IRAM/MAMBO sample of 24 M-dwarfs (Table 2), we have detected emission in form of 5 isolated sources around the M3.5 dwarf GJ 628 (Fig. 2). We have investigated whether or not these sources might simply be background galaxies. We have used the large catalogue USNO B1.0 (Monet et al. 2003) containing more that a billion objects with position uncertainties of ∼0.3″ to search for optical counterparts and summarized our results in Table 3. The only convincing association is for the source named MAMBO-W at ∼154″ West of GJ 628 in Fig. 2, based on coincidence between MAMBO and USNO positions at the 1σ level. In addition, this source MAMBO-W matches within ∼1.7σ the position of the radio source NVSS163007–123940 in the 1.4 GHz NVSS catalogue by Condon et al. (1998), if σ is the NVSS and MAMBO position uncertainties quadratically combined. Hence, we conclude that MAMBO-W is a background source identified in the visible and in the radio as a quasi-flat spectrum source from cm (NVSS: 5.6 ± 0.5 mJy) to millimeter wavelengths (this paper: ∼3.6 mJy). For the other four MAMBO sources, the likelihood of optical associations is low (position discrepancies in Table 3) and they have no radio counterpart in the NVSS catalogue. Using the density of mm background sources, 600 sources deg^{-2} for S_λ > 2 mJy at 1.2 mm, found by Voss et al. (2006), we expect 1.1 background sources over the field that includes these four sources ($r \leq 90''$, dotted circle in Fig 2). In this probability calculation, we did not include the fields of the other 23 stars observed because their maps are not as deep as the one of GJ 628. Since we observe more MAMBO sources than statistically expected from the sky background, they may be instead four dust clumps that are part of a large disk (radius ∼400 AU) surrounding the M3.5 dwarf GJ 628. In this case, their temperatures would be between 8 and 12 K and their dust

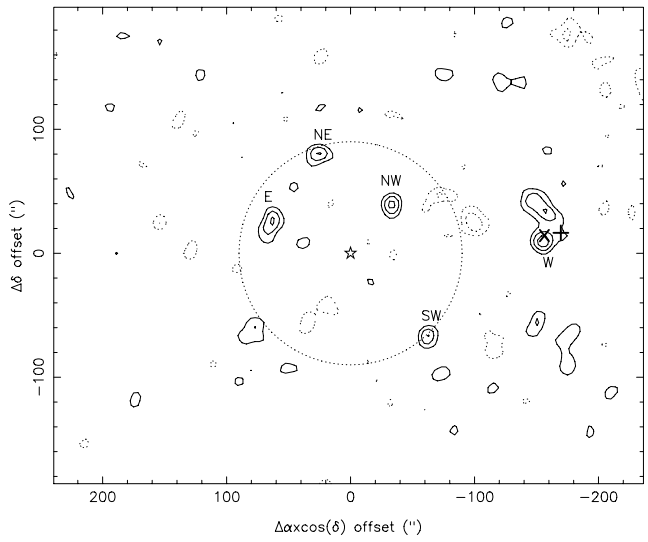

Fig. 2. IRAM/MAMBO Signal-to-Noise map of the field around the M3.5 dwarf GJ 628 at $\lambda = 1.2$ mm. In this map, Signal-to-Noise ratio (S/N) is computed from the intensity map reduced with the shift-and-add method using the software package mopsic (Zylka 1998) and smoothed to the angular resolution 12″. The S/N is computed by dividing the intensity at each pixel by the local rms (10 × 10 pixels) which is not uniform across this intensity map made by the scanning technique. The local rms σ is ∼0.4 mJy/11″ beam in the central region ($r < 60''$) and degrades towards the edges of the map; for example, 1σ is 0.75 mJy/11″ beam at $r \sim 150''$. The countours are $-3\sigma, -2\sigma$ (dotted lines), and $2\sigma, 3\sigma, 4\sigma$; The map pixel size is 3.5″. The West component (MAMBO-W) is associated with a 1.4 GHz radio source (× symbol) of the NVSS catalogue and with an optical object of the USNO-B1.1 catalogue (+ symbol), and so it is a background source. The other four MAMBO components (NW, NE, E, SW) may be dust clumps of a large debris disk around GJ 628 but the lack of diffuse emission between them requires additional observations for confirmation. Observed position of GJ 628 at center of the map is α = 16h 30m 18.0s and $\delta = -12°39'51''$ (J2000).

masses would be ∼0.1 lunar mass each. We found no significant mm diffuse emission between these point-like sources at the 0.4 mJy/11″ beam level after 20 h of integration. If GJ 628 were similar to ϵ Eri, the expected diffuse component should be seen at the 2σ level in Fig. 2. Note that close inspection of this map does show that there is a 1-σ to 2-σ emission extending between the E and NE MAMBO sources. It was not possible to image deeper with the MAMBO array in a reasonable oberving time to confirm such an extended emission. Only additional observations, in the Far-IR, in scattered light or by a long-term astrometric monitoring of the mm sources that would share the proper motion of GJ 628 (∼1.2″/yr) if they are part of its debris disk, could provide decisive evidence for this intriguing result. We don't retain GJ 628 as having a disk at this stage of our investigation.

We found the significant IRAS/*scanpi* flux densities 385 ± 21 mJy at 12 μm and 110 ± 25 mJy at 25 μm (color-corrected) for GJ 628, but they match the NextGen photospheric emission computed for this M3.5 dwarf. So no mid-IR emission excess above photospheric level is observed.

For the other stars, no emission is apparent in their MAMBO maps, and no significant mean brightness is detected when averaging the data over an effective disk with an angular diameter (θ) corresponding to the canonical diameter 120 AU, i.e. the size of the Kuiper Belt. Hence, we have used the map noise rms of each star to derive the 3-σ upper limit of its dust mass by averaging data over this canonical disk. In such a derivation, the 3σ total flux density over the effective area ($\theta(''$)) is $F_\theta = 3 \times \mathrm{rms} \times (\theta('')/11'')$ (mJy), which takes into account that the measured brightness uncertainty decreases as $\mathrm{rms}/(\theta/11'')$, i.e. as $\mathrm{rms}/\sqrt{\text{number of beams in the disk area}}$, while the total flux density increases as $(\theta/11'')^2$, i.e. as (number of beams in the disk area)^2. The dust mass is computed from this total flux density F_θ using the optically thin dust model described above substituting F_θ for S_λ and taking the absorption coefficient $\kappa_{\mathrm{abs}} = 1.3$ cm^2 g^{-1} at $\lambda = 1.2$ mm, according to the modified black-body law and $\beta = 0.8$. The implicit assumption of a disk seen face-on in this derivation provides a conservative upper limit for the total flux density and hence for the circumstellar dust mass since an inclined disk would be covered by a smaller number of beams. In Table 2, we report the values for $\theta(''$), mean brightness, brightness uncertainty, map noise rms, F_θ and dust mass upper limit. We do not confirm the 2σ flux density of 17 mJy for GJ 873 (EV Lac) at $\lambda = 1.1$ mm reported by Doyle & Mathioudakis (1991).

5. Discussion

5.1. Debris disks in our sample of 32 M-dwarfs

Our surveys of 32 young M-dwarfs conducted at $\lambda = 850\,\mu$m and 1.2 mm yielded the detection of one disk around the M0.5 dwarf GJ 842.2. The emission from this disk is a peak at 7″ South West from the star (∼140 AU at 20.9 pc) embedded in low brightness emission extending over 25″ (∼500 AU). We fitted a simple dust model by assuming large grains (∼100 μm) at mean disk radius (300 AU, 13 K) that yielded 28 ± 5 lunar masses of cold dust for the total flux density measured. No other map shows convincing evidence for a debris disk in our survey, although the SCUBA incomplete map of the M0 dwarf GJ 696 (21.9 pc) shows a localized source (11 ± 2.7 mJy) at 21″ from the star but no extended emission at the level of 0.8 mJy/14″ beam over 35″, and the MAMBO map of the M3.5 dwarf GJ 628 (4.3 pc) shows four mm sources within 90″ (400 AU) from this star but no significant diffuse emission at the 0.4 mJy/11″ beam level. We do not consider these isolated clumps as sufficient evidence for debris disks around these last two stars. However, one of the most defining features of debris disks that have been imaged in the (sub)mm is that they are not smooth, but clumpy, and so we plan other observations to investigate these cases further.

It is interesting to discuss the lifetimes of grains in the debris disk of GJ 842.2. Due to the low emission efficiency in the sub-mm of micron-sized grains, the $\lambda = 850\,\mu$m emission is expected to arise from grains larger than 100 μm (Wyatt & Dent 2002). Their collisional lifetime is $t_{\mathrm{coll}} \geq 250$ Myr and their Poynting-Robertson (P-R) drag lifetime ≥ 22 Gyr at distance $r \geq 140$ AU. These lifetimes are larger than the star age (200 Myr) and so it means that these large grains at $r \geq 140$ AU could be original ("primordial") from the early protoplanetary phase. On the other hand, grains closer to the star than 140 AU, if any, could not be primordial because of their shorter t_{coll}, i.e. more frequent constructive or destructive collisions. The large disk around GJ 842.2 is thus unique in terms of the possible presence of primordial and processed large dust grains at such a late stage of evolution and implies a large protoplanetary disk at birth. Previous to our survey, only the field M-dwarfs AU Mic and GJ 182 were detected in the sub-mm (Liu et al. 2004). These two stars are 10–20 Myr old (see Favata et al. 1998; and Barrado y Navascues et al. 1999, for the age of GJ 182). The disk of AU Mic was resolved by several workers (Kalas et al. 2004;

Table 3. Positions of the five IRAM/MAMBO sources in the map of GJ 628 at λ = 1.2 mm (Fig. 2) and their nearest optical objects referenced in the USNO-B1.0 catalogue.

	MAMBO					USNO-B1.0	
Name	α^a (J2000)	δ^a (J2000)	Flux^b density (mJy)	Star-source separation ($''$) (AU)		Object-source separation ($''$)	Object magnitudes
MAMBO-W	16 30 07.5	−12 39 42	3.6	154	660	3.0 (1.0σ)	B = 20.03 R = 19.12
MAMBO-NW	16 30 15.6	−12 39 11	2.7	53	230	13.3 (4.0σ)	B = 20.50 R = 17.90
MAMBO-SW	16 30 13.9	−12 39 59	2.0	90	390	10.1 (3.0σ)	B = 19.27 R = 18.23
MAMBO-NE	16 30 19.7	−12 39 32	2.4	83	360	9.1 (2.5σ)	B = 20.06 R = 18.30
MAMBO-E	16 30 22.3	−12 39 25	1.8	68	290	6.9 (2.0σ)	B = 21.63 I = 18.61

[a] The coordinates uncertainties are 3.5$''$ for MAMBO. [b] Flux densities are the peak values unaffected by Gaussian smoothing of the map.

Table 4. Dust masses of debris disks around A- to K-type main sequence stars. Note that HD 34700 and HD 39944 previously classified as debris disks have been rejected; HD 34700 is a T Tauri (Sterzik et al. 2005) and has gas emission (Dent et al. 2005) and HD 39944 was confused with a background galaxy (Moór et al. 2006).

Star	Sp. type	dist (pc)	age (Myr)	S_ν (mJy)	λ (mm)	Disk radius (AU)	Dust temp (K)	Dust mass (moon)
τ Ceti	G8V	3.65	10000	4.6 ± 0.6[a]	0.85	55	40	0.04
ϵ Eri	K2V	3.22	730	40 ± 1.5[b]	0.85	60	37	0.26
GL 182	M0.5	26.7	20–150	4.8 ± 1.2[c]	0.85	60	27	3.35
HD 104860	F8	47.9	40	6.8 ± 1.2[d]	0.85	60	49	7.1
HD 8907	F8	34.2	180	4.8 ± 1.2[d]	0.85	60	49	2.6
β Pic	A5V	19.3	12	104 ± 10[e]	0.85	60	77	11
HD 38393	F7V	8.97	1660	2.4 ± 1.0[f]	0.85	200	31	0.15
HD 48682	G0V	16.5	3300	5.5 ± 1.0[f]	0.85	110	38	0.9
HD 74067B	A2V	30	63	7.2 ± 1.5[h]	0.85	60	92	1.4
HD 99803B	A3V	100	123	4.7 ± 1.6[h]	0.85	60	86	11.3
HD 107146	G2V	28.5	80	20 ± 4[i]	0.85	60	47	7.8
η Corvi	F2V	18.2	1000	14.1 ± 1.8[m]	0.85	150	43	2.5
HD 112412	F1	25	28	3.8 ± 1.1[h]	0.85	60	64	0.8
HD 128167	F2V	15.5	1700	6.2 ± 1.7[f]	0.85	320	31	1.2
HD 131156	G4V	6.70	200	6.2 ± 1.9[j]	1.30	60	45	0.4
Vega	A0V	7.76	350	45.7 ± 5.4[f]	0.85	70	97	0.6
AU Mic	M1	9.9	12	14.4 ± 1.8[c]	0.85	40	31	1.2
Fomalhaut	A3V	7.69	280	97 ± 5[f]	0.85	80	61	1.6
HD 218396	A5V	40	n/a	28 ± 11[k]	1.10	60	77	24.6

[a] Greaves et al. (2004); [b] Greaves et al. (1998); [c] Liu et al. (2004); [d] Najita & Williams (2005); [e] Zuckerman et al. (1993); [f] Sheret et al. (2004); [h] Wyatt et al. (2003); [i] Williams et al. (2004); [j] Holmes et al. (2003); [k] Sylvester et al. (1996); [l] Wilner et al. (2003); [m] Wyatt et al. (2005).

Liu 2004; Krist et al. 2005) that found the size ∼200 AU smaller than the one for GJ 842.2 while these two stars have the same spectral type but one is twenty times younger. Further investigations should attempt to establish whether the environmental factor or the evolutionary factor controls these two disks.

Plavchan et al. (2005) have not detected any warm debris disks via 11 μm excess in their sample of 9 M-dwarfs older than 10 Myr. These authors highlight that stellar wind drag rather than P-R drag is responsible for dispersal of the dust in these systems and this might explain the dearth of debris disks around M-dwarfs. For GJ 842.2 ($L_* = 0.063\ L_\odot$), a stellar wind with a mass-loss rate $\dot{M}_{\rm sw}$ 20 times the solar rate ($\dot{M}_\odot \sim 2 \times 10^{-14}\ M_\odot$/yr) would be sufficient to remove the primordial grains of its disk in 200 Myr according to the P-R to stellar wind drag timescales ratio $t_{\rm PR}/t_{\rm sw} \propto \dot{M}_{\rm sw}/L_*$ (Eq. (3) of Plavchan et al. 2005). In fact, winds with mass-loss rates 1000 times the solar rate are observed for M-dwarfs, especially when young, and would make the existence of primordial dust after 200 Myr inconceivable. Unfortunately, no X-ray or CaII data are available that would allow an estimate of $\dot{M}_{\rm sw}$ for GJ 842.2. However, GJ 842.2 is not a flare star, and its H_α absorption (equivalent width $EW_{H_\alpha} = -0.545$ Å, in Gizis et al. 2002) indicates a moderate chromosphere and magnetic activity, and thus only a modest stellar wind (Mullan et al. 1992, 2001, and Wargelin & Drake 2001). Hence, one can speculate that GJ 842.2 does not have a mass-loss rate larger than 20 times the solar rate and its distant cold grains are unperturbed at age 200 Myr. Although GJ 628 is not retained as having a debris disk in the present analysis, it is interesting to note that its X-ray luminosity ($10^{26.79}$ erg s^{-1} measured by ROSAT, et al. 2004) is low, similar to that of the quiet Sun ($10^{26.5}$ erg s^{-1}), and its EW_{H_α} (−0.234 Å, in Gizis, et al. 2002) indicates a weak to moderate chromosphere. Hence, similarly to GJ 842.2, if GJ 628 were surrounded by cold grains, one can speculate that they would be unperturbed at age 20–150 Myr. Finally, we note also that there is no difference in disk detection rates between the subsample of 11 stars with high L_x (i.e. Log (L_x) > 27.5) and the subsample of 7 stars with low L_x in Tables 1 and 2.

We have critically reviewed the literature to list the properties of the debris disks around A- to K-type main sequence stars in Table 4 and plotted their dust masses as a function of spectral types in Fig 3 after adding our results for the M-dwarfs. The 200 Myr old debris disk around GJ 842.2 is relatively massive (28 lunar mass of dust) and may be the tip of the iceberg for the

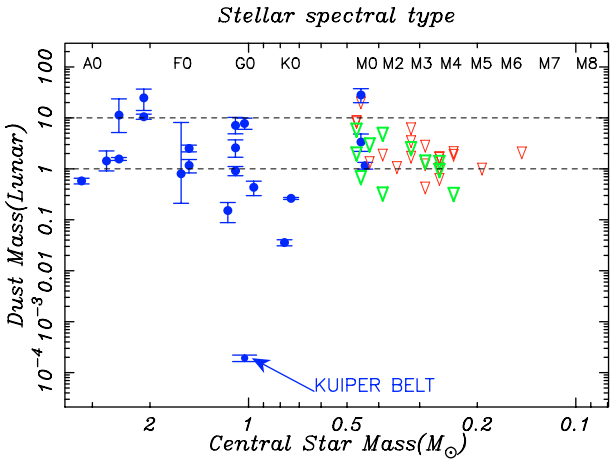

Fig. 3. Dust masses of debris disks (filled circles) around A- to K-type main sequence stars (Table 4), around the two M-dwarfs AU Mic and GL 182 from Liu et al. (2004) and around the M-dwarf GJ 842.2 reported in this paper. In addition, we plot the dust mass 3σ upper limits of potential disks for the non-detections of this paper and for the M-dwarf GJ 799 reported in Liu et al. (2004) (red thin triangles = SCUBA and green thick triangles = MAMBO). The dust mass for the Kuiper Belt is shown here to indicate that present observations provide dust masses that are only the envelope of a possibly much larger population of debris disks. The dashed lines are plotted as a guide.

M-dwarf disks. We note that this mass is comparable to the highest disk mass of the A- to K-type main sequence stars plotted in Fig. 3. Future surveys will have to establish whether or not this upper envelope for the non-detected M-dwarfs in Fig. 3 is a real envelope to assert whether or not disks around M-dwarfs are as massive as around A- to K-type stars. Presently, this comparison is also complicated by the fact that the debris disks detected in the (sub)mm around these A- to K-type stars are from an IRAS-selected sample from essentially an all-sky survey, while the M-dwarfs in our analysis are from an unbiased (except for age) sample of 32 stars. Eventually, a broader comparison with protoplanetary disk masses and central star masses (Natta et al. 2000 and Andrews & Williams 2005) will allow to discuss how the mass of the central star impacts planet formation.

5.2. Detection rate of dusty debris disks around M-dwarfs

We have combined our surveys (32 field M-dwarfs observed and 1 detection) with the JCMT survey of 3 field M-dwarfs with 2 detections by Liu et al. (2004). Note that their small sample has the same characteristics in ages, distances and sensitivity as ours; AU Mic (9.9 pc) and GJ 799 (10.3 pc) of the β Pic moving group (age 10–20 Myr) and GJ 182 (26 pc) of the Local Association. In this combination, there are (1 + 2) detections out of (32 + 3) M-dwarfs searched, yielding the detection rate $f = 8^{+4}_{-6}\%$ for cold debris disks in this sample of M-dwarfs with ages between 20 and 600 Myr observed in the (sub)mm. We have derived the uncertainty by computing the full width half maximum of the probability distribution $P(k/N) = C^k_n(1-f)^{N-k}f^k$ that k detections be found in a sample of N stars searched if the a priori frequency of occurence is f.

In order to compare detection rates between surveys, it is important to compare observations in the same wavelength regime since mid-IR surveys probe warm dust (~100 K) close to the star (~1 AU) while (sub)mm surveys probe cold dust (~20 K) distant from the star (100's AU). In the literature, there are two surveys of A- to K-type stars conducted in the sub-mm that are suited for comparison with our detection rate. A sample of A- and F-type main sequence stars not detected by IRAS with ages 10–170 Myr was conducted at 850 μm by Wyatt et al. (2003) and a sample of F- to K-type stars with ages 10–180 Myr was conducted at 850 μm by Najita & Williams (2005). It is important also to trim the samples so that they have same age interval since the decay of dust in debris disks with time seen for A-type stars (Rieke et al. 2005) is likely to affect M-dwarfs too. For these considerations, we therefore have restricted our (sub)mm sample to the (3 + 20) M-dwarfs with ages 20–200 Myr, including the three M-dwarfs studied by Liu et al. (2004) satisfying this age limit. We then find that our detection rate f becomes $13^{+6}_{-8}\%$ (3/23) for cold debris disks surrounding field M-dwarfs with ages between 20 and 200 Myr. This detection rate f compares well with the detection rate (9–14%) found in the A- and F-type star sample of Wyatt et al. (2003), and to the detection rate $23^{+13}_{-15}\%$ (3 detections for 13 stars observed) in the F- to K- type star sample of Najita & Williams (2005). It is remarkable that these cold dust detection rates for M-dwarfs and A- to K-type dwarfs match. This may indicate that the populations of cold debris disks among early and late-type stars are alike. We have also considered the sub-sample of 89 F- to K-type stars with ages between 10 and 300 Myr observed at λ = 1.2 mm, 2.7 mm and 3 mm by Carpenter et al. (2005) that has a detection rate of 2%. It is somewhat lower than the rates above but the longer wavelengths used in their observations would have required deeper observations to be directly comparable to the other surveys.

6. Conclusions

We have searched for cold debris disks around 32 field M-dwarfs at sub-mm and mm wavelengths. We report evidence for a new debris disk around the M0.5 dwarf GJ 842.2 of age ~200 Myr which is massive (28 ± 5 lunar masses) and large (~500 AU). We report also the detection of four mJy sources at 1.2 mm around the M3.5 dwarf GJ 628 that might be associated with a debris disk around this star unless they are background sources.

By combining the result of our surveys with the two cold debris disks discovered by Liu et al. (2004) in their observations of three field M-dwarfs, we derive for the first time the detection rate $f = 13^{+6}_{-8}\%$ for cold debris disks surrounding M-dwarfs with ages 20–200 Myr. This detection rate for M-dwarfs is consistent with the detection rate 9–23% for cold disks around A- to K-type main-sequence stars with ages 10–180 Myr measured by Wyatt, et al. (2003) and Najita & Williams (2005) in two sub-mm surveys. The consistency between these detection rates is the first indication that a population of cold disks is equally prevalent across stellar spectral types. The highest disk mass (28 ± 5 lunar masses for GJ 842.2) among the M-dwarfs is comparable to the highest disk mass among the A- to K-type main sequence stars (Table 4 and Fig. 3). We plan additional observations of a larger sample of M-dwarfs to ascertain this detection rate and to better determine the dust mass upper envelope of field M-dwarfs. The dust mass for the Kuiper Belt is $\sim 3 \times 10^{-4}$ lunar mass (Landgraf et al. 2002; and Moro-Martín & Malhotra 2003), and, clearly, deeper observations are required to establish the statistics of debris disks around mature stars over a large range of ages.

Acknowledgements. We are grateful to the staffs of the JCMT and of the IRAM 30-m telescope for their dedication in carrying out the observations reported in this publication. The JCMT project number was m04bu06. This research has made use of the SIMBAD database and of the VizieR catalog access tool, operated at the Centre de Données Stellaires (CDS), Strasbourg, France. This publication makes use of data products from the Two Micron All Sky Survey, from IRAS and Scanpi Processing maintained at the Infrared Processing and Analysis Center (IPAC), California Institute of Technology, Pasadena, CA.

References

Allard, F., Hauschildt, P. H., & Schwenke, D. 2000, ApJ, 540, 1005
Allard, F., Hauschildt, P. H., Alexander, D. R., Tamanai, A., & Schweitzer, A. 2001, ApJ, 556, 357
Andrews, S. M., & Williams, J. P. 2005, ApJ, 631, 1134
Aumann, H. H., Beichman, C. A., Gillett, F. C., et al. 1984, ApJ, 278, L23-27
Backman D. E., & Paresce, F. 1993, in Protostars and Planets III, ed. E. H. Levy & J. I. Lumine (Tucson: Univ. Press), 1253
Barrado y Navascués, D., Stauffer, J. R., Inseok Song, & Caillault, J.-P. 1999, ApJ, 520, L123
Beaulieu, J.-P., Bennett, D. P., Fouqué, P., et al. 2006, Nature, 439, 437
Beckwith, S. V. W., Sargent, A. I., Chini, R. S. & Güsten, R. 1990, AJ, 99, 924
Beichman, C. A., Bryden, G., Rieke, G. H., et al. 2005, ApJ, 622, 1160
Beichman, C. A., Tanner, A., Bryden, G., et al. 2006, ApJ, 639, 1166
Bonfils, X., Forveille, T., Delfosse, X., et al. 2005, A&A, 443, L15
Bryden, G., Beichman, C. A., Trilling, D. E., et al. 2006, ApJ, 636, 1098
Butler, R. P., Vogt, S. S., Marcy, G. W., et al. 2004, ApJ, 617, 580
Carpenter, J. M., Wolf, S., Schreyer, K., Launhardt, R., & Henning, T. 2005, AJ, 129, 1049
Chen, C. H., Patten, B. M., Werner, M. W., et al. 2005, ApJ, 634, 1372
Condon, J. J., Cotton, W. D., Greisen, E. W., et al. 1998, AJ, 115, 1693
Dent, W. R. F., Walker, H. J., Holland, W. S., & Greaves, J. S. 2000, MNRAS, 314, 702
Dent, W. R. F., Greaves, J. S., & Coulson, I. M. 2005, MNRAS, 359, 663
Doyle, J. G., & Mathioudakis, M. 1991, A&A, 241, L41
Dutrey, A., Guilloteau, S., Duvert, G., et al. 1996, A&A, 309, 493
Endl, M., Cochran, W. D., Tull, R. G., & MacQueen, P. J. 2003, AJ, 126, 3099
Favata, F., Micela, G., Sciortino, S., & D'Antona, F. 1998, A&A, 335, 218
Gaudi, B. S., et al. 2002, ApJ, 566, 453
Gizis, J. E., Reid, I. N., & Hawley, S. L. 2002, AJ, 123, 3356
Golimowski, D. A., Ardila, D. R., Krist, J. E., et al. 2006, AJ, 131, 3109
Greaves, J. S., Holland, W. S., Moriarty-Schieven, G., et al. 1998, ApJ, 506, L133
Greaves, J. S. Wyatt, M. C., Holland, W. S., Dent, W. R. F., et al. 2004, MNRAS, 351, 54
Greaves, J. S., Holland, W. S., Wyatt, M. C., et al. 2005, ApJ, 619, 187
Habing, H. J., Dominik, C., Jourdain de Muizon, M., et al. 2001, A&A, 365, 545
Haisch, K. E., Lada, E. A., & Lada, C. J. 2001, ApJ, 553, L153
Holland, W. S., Greaves, J. S., Zuckerman, B., et al. 1998, Nature, 392, 788
Holland, W. S., Robson, E. I., Gear, W. K., et al. 1999, MNRAS, 303, 659
Holmes, E. K., Butner, H. M., Fajardo-Acosta, S. B., & Rebull, C. R. 2003, AJ, 125, 3334
Huensch M., Schmitt J. H. M. M., Sterzik M. F., Voges W. 1999, A&AS 135, 319
Inseok Song, Weinberger, A. J., Becklin, E. E., Zuckerman, B., & Chen, C. 2002, AJ, 124, 514
Jenness, T., Stevens, J. A., Archibald, E. N., et al. 2002, MNRAS, 336, 14
Johnstone, D., Hollenbach, D., & Bally, J. 1998, ApJ, 499, 758
Kalas, P., Liu, M. C., Matthews, B. C. 2004, Science, 302 1990
King, J. R., Villarreal, A. R., Soderblom, D. R., Gulliver, A. F., & Adelman, S. J. 2003, AJ, 125, 1980-2017
Kreysa, E., Gemuend, H.-P., Gromke, J., et al. 1998, Proc. SPIE, 3357, 319
Krist, J. E., Ardila, D. R., Golimowski, D. A., et al. 2005, A. J., 129, 1008
Landgraf, M. Liou, J.-C., Zook, H. A., Grün, E. et al. 2002, AJ, 123, 2857
Laughlin, G., Bodenheimer, P., & Adams, F. C. 2004, ApJ, 612, L73
Laureijs, R. J., Jourdain de Muizon, M., Leech, K., et al. 2002, A&A, 387, 285
Liu, M. C. 2004, Science, 305, 1442
Liu, M. C. Matthews, B. C., Williams, J. P., Kalas, P. G. 2004, ApJ, 608, 526
López-Santiago, J., Montes, D., Crespo-Chacon, I., & Fernández-Figueroa, M. J. 2006, ApJ, 643, 1160.
Luhman, K. L., Stauffer, J. R., & Mamajek, E. E. 2005, ApJ, 628, L69-L72
Mannings, V., & Barlow, M. J. 1998, ApJ, 497, 330
Marcy, G., Fischer, D., Vogt, S. S., Lissauer, J. J., & Rivera, E. J. 2001, ApJ, 556, 296
Monet, D. G., Levine S. E., Cazian B., et al. 2003, AJ., 125, 984
Montes, D., López-Santiago, J., Gálvez, M. C., et al. 2001, MNRAS, 328, 45
Moór, A., Abrahám, P., Derekas, A., et al. 2006, ApJ, 644, 525
Moro-Martín, A., & Malhotra, R. 2003, AJ, 125, 2255
Mullan, D. J., & MacDonald, J. 2001, ApJ, 559, 353
Mullan, D. J. Doyle, J. G., Redman, R. O., Mathioudakis, M. 1992, ApJ, 397, 225
Muzerolle, J., Adame, L., D'Alessio, P., et al. 2006, ApJ, 643, 1003
Najita, J., & Williams, J. P. 2005, ApJ, 635, 625
Natta, A., Grinin, V., & Mannings, V. 2000, in Ptotostars and Planets IV, Book (Tucson: University of Arizona Press), 559
Plavchan, P., Jura, M., & Lipscy, S. J. 2005, ApJ,631,1161
Rieke, G. H., Su, K. Y. L., Stansberry, J. A., et al. 2005, ApJ, 620, 1010.
Rowan-Robinson, M. 2001, ApJ, 549, 745
Schmitt, J. H. M. M., & Liefke, C. 2004, A&A, 417, 651
Sheret, I., Dent, W. R. F., & Wyatt, M. C. 2004, MNRAS, 348, 1282
Siess, L., Dufour, E., & Forestini, M. 2000, A&A, 358,593
Skrutskie, M. F., Cutri, R. M., Stiening, R., et al. 2006, AJ, 131, 1163.
Spangler, C., Sargent, A. I., Silverstone, M. D., Becklin, E. E., & Zuckerman, B. 2001, ApJ, 555, 932.
Sterzik, M. F., Melo, C. H. F., Tokorinin, A. A., & van der Bliek, N. 2005, A&A, 434, 67
Sylvester, R. J., Skinner, C. J., Barlow, M. J., & Mannings, V. 1996, MNRAS, 279, 915.
Sylvester, R. J., Dunkin, S. K., Barlow, M. J. et al. 2001, MNRAS, 327, 133.
Throop, H. B., & Bally, J. 2005, ApJ, 623, L149.
Voss, H., Bertoldi, F., Carilli, C., et al. 2006, A&A, 448, 823
Wargelin, B. J., & Drake, J. J. 2001, ApJ, 546, 57
Williams, J. P. Najita, J., Liu, M. C., et al. 2004, ApJ, 604, 414
Wilner, D. J., Holman, M. J., Kuchner, M. J., Ho, P. T. P. 2003, ApJ, 596, 597
Wyatt, M. C. 2003, ApJ, 598, 1321
Wyatt, M. C., Dent, W. R. F. 2002, MNRAS, 334, 589
Wyatt, M. C., Dent, W. R. F., Greaves, J. S. 2003, MNRAS, 342, 876
Wyatt, M. C., Greaves, J. S., Dent, W. R. F., & Coulson, I. M. 2005, ApJ, 620, 492
Walker, H. J., & Wolstencroft, R. D. 1988, PASP, 100, 1509.
Zuckerman, B., & Becklin, E. E. 1993, ApJ, 414, 793
Zuckerman, B., & Inseok Song 2004a, ARA&A, 42, 685
Zuckerman, B., & Inseok Song 2004b, ApJ, 613, L65
Zylka, R., `http://www.iram.es/IRAMES/otherDocuments/ manuals/Datared/`